Synthesis and characterization of squaramide-based supramolecular polymers

Lauria, F.

CHAPTER 5

Visible light crosslinking of squaramide-based supramolecular polymers through tyrosine cross-linking

5.1 Abstract

Supramolecular materials that are held together by non-covalent interactions are gaining remarkable attention in the biomedical field for their capacity to mimic structural and functional attributes of ECM proteins. However, in comparison to the covalent polymers that are held together with largely irreversible bonds, supramolecular materials display weak mechanical properties that limit their applications. A powerful strategy to tune the mechanical properties of the resultant self-assembled materials is through the application of covalent crosslinks. When photoreactive groups are used, spatiotemporal control over materials properties can be achieved using light as an external stimulus. We herein examine the inclusion of tyrosine moieties into a squaramide-based supramolecular monomer to enable its visible light crosslinking. More specifically, a tyrosine dipeptide-functionalized squaramide-based monomer was synthesized to obtain supramolecular polymers and its visible light cross-linking with the use of FMN and $Ru(bpy)_3^{2+}$ photoinitiators to prepare gel materials is disclosed.

5.2 Introduction

Functional supramolecular hydrogels based on peptides are considered as promising candidates for tissue engineering and regenerative medicine because of their biocompatible and biodegradable nature.[1–5] Moreover, their self-assembly starting from small molecules provide numerous opportunities to modulate the properties of the formed materials based on the features of the designed monomer, namely its sequence.[6,7] The amino acid sequence with the relative positioning of the units dictates the non-covalent interactions (e.g. π-π stacking, hydrogen bonding and hydrophobic interactions) that will work together to form the polymers.[8,9] Short peptide sequences involving two, three or four amino acids have shown the ability to form a diverse array of filamentous nanostructures and hydrogel materials.[6,10,11] Often their design is based on sequences containing aromatic units (e.g. Phe, Tyr) and can include larger non-amino acid units (e.g. Fmoc).[12–14] However, a major challenge for these materials once assembled is their weak mechanical properties that limit their application in the biomedical area, thus further tuning of their properties on self-assembly is necessary. One strategy to improve the properties of these materials is to introduce units that would enable their covalent crosslinking under cell culture conditions. Such crosslinking has been achieved using various conjugation chemistries such as Schiff-base, hydrazone, acylhydrazone, Diels-Alder, and disulfide, and thiol-ene reactions.[12,15–18] However, the use of light activatable chemistries is highly attractive as it provides opportunities for spatiotemporal control of mechanics and bioactivity of these materials.

UV or visible light have been used to stimulate photocrosslinking in covalent polymer hydrogels with the aid of a photoinitiator.[19,20] Photoinitiators such as lithium phenyl-2,4,6-trimethylbenzoylphosphinate (LAP), flavin mononucleotide (FMN), Eosin-Y and tris(bipyridine)ruthenium(II) $[Ru(bpy)_3]^{2+}$ have been used to provide a radical source to trigger crosslinking. More recently, visible light photoinitiators (e.g. FMN, $Ru(bpy)_3^{2+}$) have been examined to crosslink of phenol-based molecules (e.g. tyrosine) in peptide and polymer materials for a range of 3D cell culture applications, including bioprinting. Tyrosine dimerization can be easily followed with the characteristic absorption and emission of dityrosine (λ_{abs} = 320 nm; λ_{em} = 420 nm) as compared to the unreacted amino acid (λ_{abs} = 280 nm; λ_{em} = 305 nm).[21,22] In a PEG-peptide hydrogel containing tyrosine (e.g., CYGGGYC), the mechanical properties were modulated by the time of light exposure, FMN concentration and number tyrosine residues.[22] Importantly, tyrosine

interactions play an important role in stabilizing natural materials such as resilin, silk, alginate, and collagen.[23–27] The biological relevance of these bonds and their crosslinking at visible wavelengths that can be more cytocompatible make them attractive for use in tissue culture,[28] and thus we became interested in their use to tune the self-assembly behaviour of supramolecular polymers.

We previously reported supramolecular materials based on a tripodal squaramide-based monomer for 3D cell culture applications.[29–31] The hydrogels are soft (<100 Pa in storage modulus, G'), but the lack of chemical handle precludes their further crosslinking. In the previous chapter, we found that even removal of one squaramide moiety from the core and further modulating the hydrophilic-hydrophobic balance can result in gels. In this monomer, two strategies can be envisaged to introduce a tyrosine moiety in these monomers; either on the periphery of each arm of the monomer, or through substitution of one squaramide arm with a tethered tyrosine moiety. We opted for removal of one squaramide arm because of the solubility of the tyrosine and bridged its attachment to the squaramide core with a tetraethylene glycol chain. Herein, we prepare the tyrosine dipeptide outfitted monomers with and without carbamate linkages (Scheme 1) and examine its self-assembly and crosslinking with an FMN photoinitator in the visible light range.

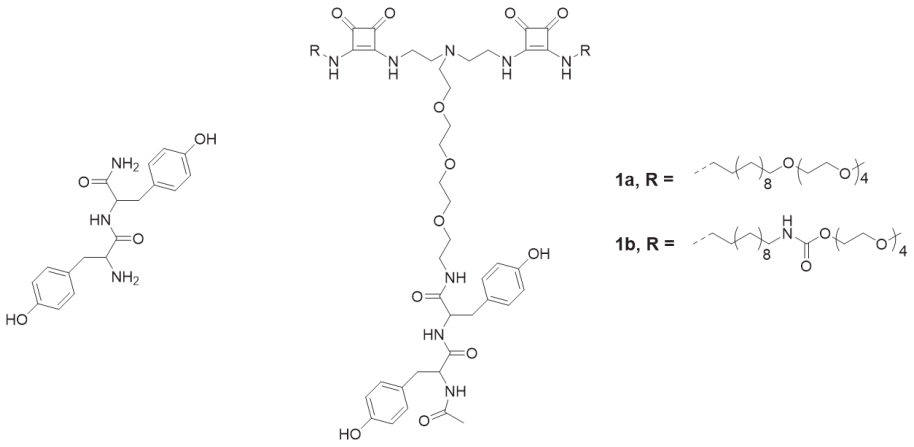

Scheme 1: Chemical structures of tyrosine dipeptide and tyrosine dipeptide-coupled squaramide monomer with (**1a**) and without (**1b**) peripheral carbamate linkage.

5.3 Results and discussion

In chapter 4, we found that removing one squaramide arm from a tripodal squaramide derivative and the addition of a tetraethylene glycol chain results in a lack of aggregation on self-assembly as consequence of its increased hydrophilic character. We selected this monomer because of the hydrophobic nature of the dityrosine that is expected to increase on self-assembly and after light-mediated crosslinking.

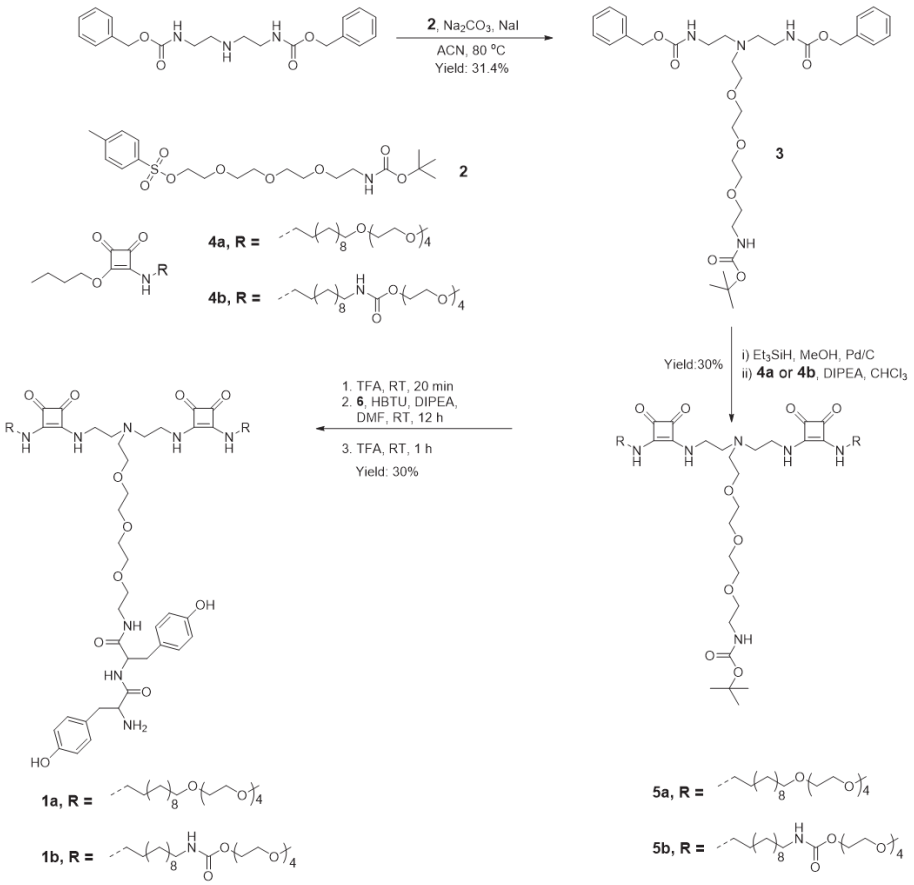

Scheme 2. Synthetic route to tyrosine dipeptide-coupled squaramide-based monomer **1a** and **1b**.

Moreover, the tyrosine dipeptide has also been reported to self-assemble on its own into nanofibers[23] (Scheme 1). Though a single tyrosine moiety is sufficient cross-linking, we applied the tyrosine dipeptide to additionally benefit from the potential synergistic effect of the self-assembly of the dipeptide that could influence the squaramide supramolecular polymer structure prior to crosslinking. We examine the effect of its conjugation to squaramide monomers (**1a** and **1b**) on modulating the self-assembly before and after visible light irradiation.

The tyrosine dipeptide-coupled squaramide-based monomers, **1a** and **1b**, were synthesized through a multistep reaction sequence as shown in Scheme 2. Initially, compound **6** was synthesized by reacting Ac-O-(*tert*-butyl)-L-tyrosine with O-(*tert*-butyl)-L-tyrosine via DCC/NHS coupling in DMF with 75% yield. The heterobifunctional tetraethyleneglycol (**2**), squaramide amphiphile with a decyl spacer and a carbamate (**4a**) and without carbamate group (**4b**) were separately synthesized using literature reported procedures.[32] The synthesis of tripodal amphiphiles commenced with the reaction of *N*,*N*″-di-Z-diethylenetriamine with **2** in the presence of sodium carbonate to provide **3** in 31% yield. The Cbz group was subsequently deprotected by *in situ* hydrogenation with triethylsilane on activated palladium and substituted with squaramide units to yield **5a** (30%) and **5b** (28%). The product was further treated with 50% trifluoroacetic acid in chloroform for boc-deprotection and then coupled with tyrosine dipeptide using HBTU in DMF. The final product was isolated after deprotection of the tert-butyl group using TFA at RT to yield **1a** (57%) and **1b** (30%).

To understand the changes in the assembly of the supramolecular induced by the conjugation of the tyrosine dipeptide, AFM experiments were performed. When the tyrosine peptide is conjugated to the tripodal squaramide-based supramolecular monomer, **1a**, spherical aggregates are were observed on dilution from a 1 mM stock solution on mica (15 μM) (**Figure 2a**). The lack of aggregates with a fibrillar morphology could be due to the position of the hydrophilic domain in the monomer structure, as it is conjugated to the central nitrogen in the monomer core and can hinder the formation of the other non-covalent interactions between monomers.

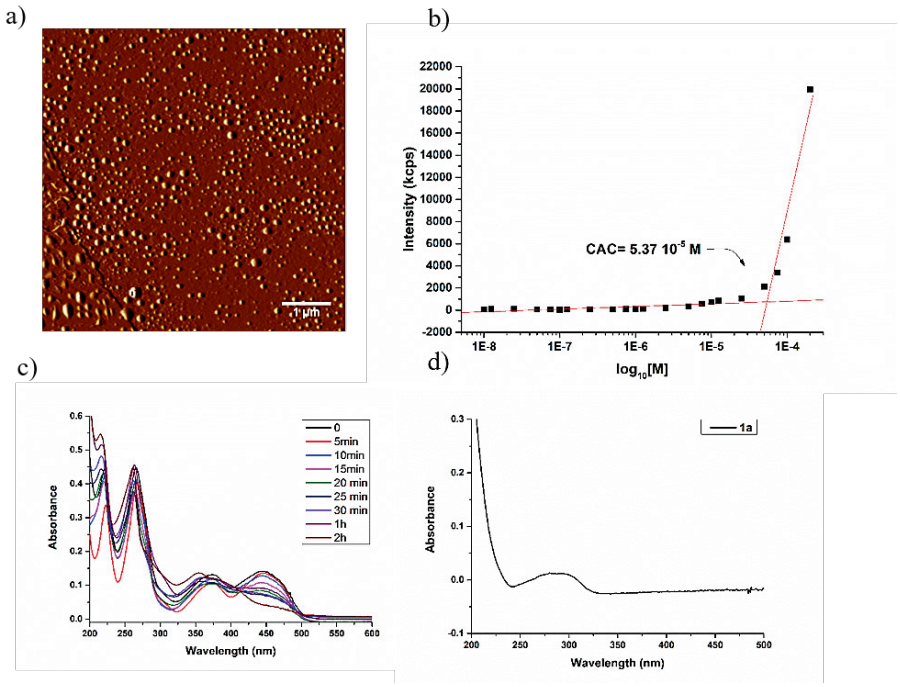

Figure 2 (a) AFM micrographs of **1a**, stock solution 1 mM diluted to 15 µM (scale bar = 1 µm) (b) Critical aggregation concentration of **1a** by static light scattering (SLS) ; (c) UV-vis spectra of **1a** (1 mM diluted to 15 µM); in presence of FMN (15 µM) at different irradiation times at 450 nm; d) UV-vis spectrum of **1a** (15 µM).

The self-assembly of **1a** at the molecular level was further evaluated by UV-vis spectroscopy. A broad absorption band between 250-320 nm lacking the characteristic red- and blue-shifting of the HOMO-LUMO and HOMO-LUMO+1 transitions of squaramide synthon on self-assembly was observed (**Figure 2d**). Combined with the observations in AFM imaging, namely the formation of spherical aggregates, these results point to monomer **1a** being unable to form fibrillar aggregates at the tested concentration. Despite earlier reports that show the formation of supramolecular polymers from tyrosine dipeptides,[23] this result suggests that the aliphatic spacer between TREN core and peptide is likely necessary for the retention of one-dimensional nanostructures at monomer concentrations in the low micromolar range, as observed for other tripodal monomers reported in Chapter 4. Moreover, the self-assembly of **1a** was further investigated by SLS (static light scattering) to determine the critical aggregation concentration (CAC) or the concentration above which the supramolecular polymers are formed (**Figure 2b**). The CAC

of **1a**, was determined from the inflection point of the scattered intensities of monomer solutions between 100 μM and 10 nM and was comparable to that one previously calculated for the compound **2a** (chapter 4, 2.13 x 10^{-5} M), further confirming the approach of self-assembly at a higher monomer concentration and its subsequent dilution for analysis.

Once aggregation behavior of the monomer was assessed, the potential of the tyrosine dipeptide unit to undergo cross-linking with visible light irradiation (λ = 440 nm) was examined. Using conditions reported by Liu *et al.*,[33] compound **1a** (1 mM) above the CAC was irradiated with visible light at 440 nm in the presence of the FMN photoinitiator at a 1 mM concentration with different irradiation times (0, 5, 10, 15, 20, 25, 30, 60 and 120 min). It was previously reported that the formation of tyrosine dimers could be identified by the growth of a new UV-vis band at 330 nm and a fluorescent signal at 420 nm.[21] Therefore, we collected UV-vis and fluorescence spectra of **1a** in the presence of FMN (1 mM) before and after being irradiated with visible light for different irradiation times until when no further spectral changes were observed (**Figure 2d**). The UV-vis profile before irradiation (t = 0 min) displayed bands at 255, 370 and 450 nm, which are consistent with the characteristic absorption of the FMN photoinitiator.[34] A control sample where visible light irradiation was applied to the FMN photoinitiator in water was performed (**Figure S5.2**). With increasing the irradiation time in the experiment, a decrease in the absorption spectrum at 450 nm was observed due to the degradation of the photoinitator.[35]

To further confirm tyrosine crosslinking between squaramide monomers, emission spectra of **1a** were recorded after irradiation with visible light for various durations (**Figure 3**). In absence of visible light irradiation, the emission profile is typical of the photoinitiator (**Figure S5.3**). On the application of visible light, the initial transitions at 525 and 550 nm disappeared and a new band at 470 nm was observed. These trends matched those observed in UV-vis experiments and are consistent with the photodegradation of FMN in water as outlined by Edwards.[35–37] Both the lack of the UV-vis band at 330 nm and the fluorescent signal at 420 nm point to the inabiltity of the tyrosine dipeptide to crosslink within this supramolecular system. We postulate that this result could arise for two reasons; either the lack of 'exposure' of phenolic hydroxyl group of tyrosine to the excited photoinitiator to trigger the radical reaction or too large of a distance between tyrosines to enable crosslinking. However, we also do not rule out the monomer concentration or choice of the photoinitiator to give rise to the

observed result, as faster initiation, on the order of seconds, can be achieved with $Ru(bpy)^{3+}$.

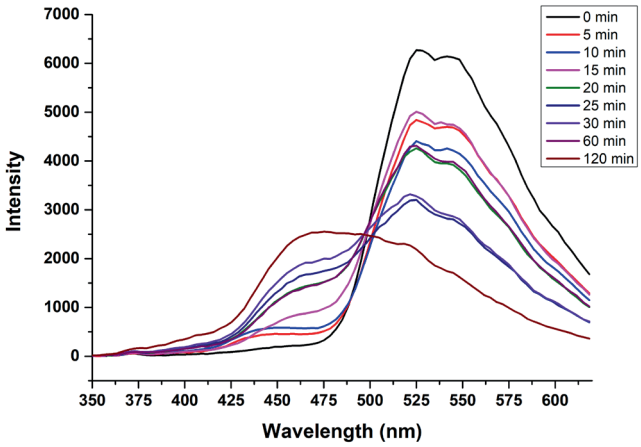

Figure 3 Emission spectra of diluted samples of **1a** (15 μM) after different visible light irradiation times (330 nm) using FMN (15 μM) as a photoinitiator. Fluorescence spectra were taken by excitation at 330 nm and collection from 350 to 620 nm.

In order to further modulate the self-assembly behaviour and photo-crosslinking of the monomer, we designed compound **1b** with a carbamate linkage at the interface of the hydrophilic and hydrophobic domains. In Chapter 4, it was demonstrated that the absence of a carbamate moiety in the tripodal squaramide monomer results in a decrease in the storage modulus (G') of the hydrogel. Therefore, the impact of using a carbamate linker on self-assembly of the tyrosine dipeptide containing monomer was examined. The UV-vis spectra on dilution of **1b** (15 μM) after self-assembly in water and CH_3CN shows a spectral profile consistent with a lack of head-to-tail aggregation of the squaramide synthons (**Figure 4a**). The slight increase in the absorption intensity in acetonitrile may be due to the increased solubility of **1b** in acetonitrile in comparison to water. Based on earlier critical aggregation concentration measurements for the ether derivative, **1a**, UV-vis spectra were taken for **1b** up to 1 mM. Upon increasing the concentration of **1b**, new absorption bands at 247 nm and 325 nm were observed (**Figure 4b**). These shifting of the HOMO-LUMO and HOMO-LUMO+1 transitions are consistent with the self-assembly of the squaramide synthon in a head-tail hydrogen bonding arrangement. The dilution of a concentrated solution of **1b**

to 0.021 mM resulted the disappearance of these bands; this concentration-dependent aggregation behaviour that can further be fit with models to gain insight into the supramolecular polymerization mechanism. DLS measurements of **1b** exhibited an increased size in water relative to acetonitrile further consistent with the formation of supramolecular polymers of **1b** in water (**Figure 4c**).

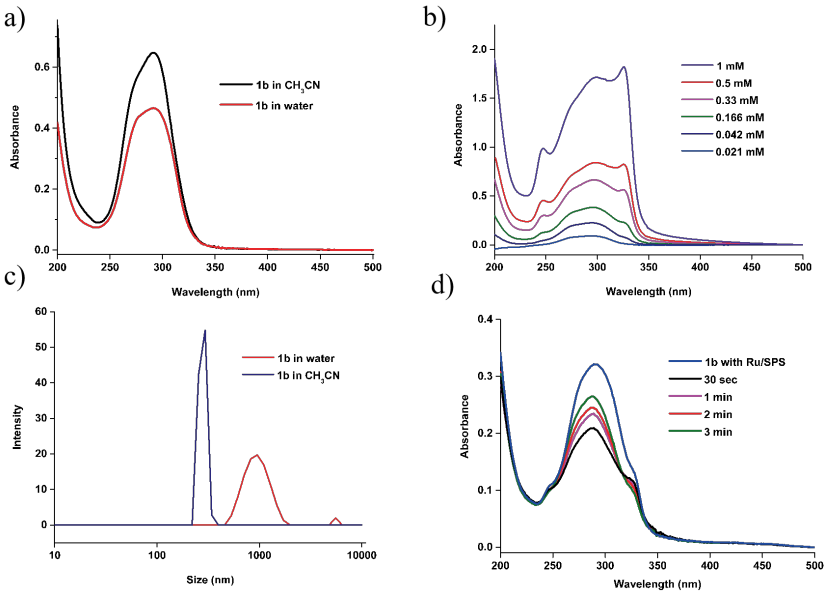

Figure 4 a) UV-vis spectra of **1b** (15 μM) in water and CH_3CN; b) Concentration-dependent absorption of **1b** in water; c) Size distribution data measured by DLS (0.166 mM) in water and CH_3CN; d) Photoirradiation of **1b** (0.166 mM) in the presence of $Ru(bpy)_3^{2+}$ (16.7 μM) and SPS (0.183 μM) using 450 nm visible light as a function of time.

Tyrosine crosslinking in supramolecular polymer **1b** was subsequently studied in the presence of $Ru(bpy)_3^{2+}$ and sodium persulfate (SPS) photoinitiators because of their capacity to enable rapid crosslinking, on the order of seconds, in the visible range at 450 nm. The concentration of **1b** was chosen at which it is in self-assembled state (0.166 mM). The photoinitiators $Ru(bpy)_3^{2+}$ (16.7 μM) and SPS (0.183 μM) were added to the solution prior to photoirradiation using 450 nm visible light. Upon photoirradiation of **1b** for 30 sec, a slight decrease in the UV absorption intensity was observed (**Figure 4d**). Extending the time of irradiation for up to 3 min resulted in an increase of the absorption band at 297 nm consistent with the monomer species and a

decrease of aggregation band at 325 nm belonging to the aggregated species. The overall decrease of the UV-vis spectra after visible light irradiation can be attributed to an increase in hydrophobicity of the cross-linked tyrosines in the supramolecular polymers. Photoirradiation of **1b** under the similar experimental conditions at low (30 µM) and high (0.5 mM) concentrations did not show any noticeable changes in the UV-vis spectra (**Figure 5a** and **5b**). As a control, a solution containing the same concentration of $Ru(bpy)_3^{2+}$ and SPS was prepared to confirm spectral changes were due to the reacted self-assembling molecules. Though it is anticipated that cross-linking of tyrosine would be highly efficient in the self-assembled state due to the close proximity of the tyrosine dipeptides on self-assembly, further investigation into the effect of self-assembly on crosslinking by varying the concentration of photoinitiator, nature of supramolecular polymers and visible light exposure time are highly necessary. While these results demonstrate that the tyrosine unit is a valid platform to modulate the self-assembly properties of supramolecular monomers, their position in the monomer structure, more specifically in their relation to their hydrophobic domains is critical for the control of supramolecular aggregates.

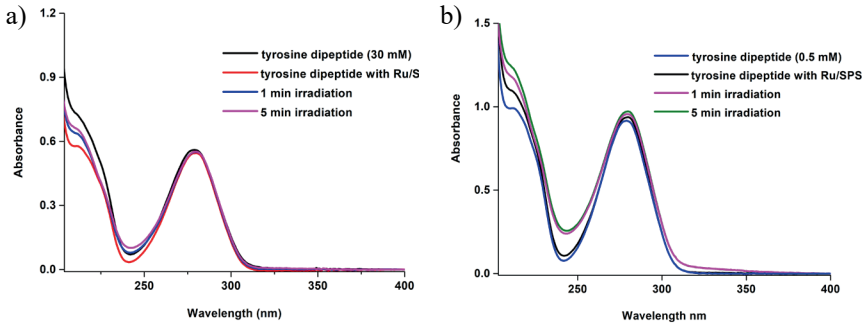

Figure 5: UV-visible spectra after photo-irradiation of tyrosine dipeptide a) at low concentration (30 µM) in the presence of $Ru(bpy)_3^{2+}$ (1.67 µM) and SPS (0.183 µM) and b) at high concentration (0.5 mM) in the presence of $Ru(bpy)_3^{2+}$ (16.7 µM) and SPS (183 µM) using 450 nm visible light as a function of time.

5.4 Conclusions

In this chapter, the effect of introducing tyrosine dipeptides on modulating the self-assembly properties of a tripodal squaramide-based supramolecular monomer was examined. Since tyrosine has been previously shown to self-assemble in nanofibers, we investigated if this self-assembling unit can influence the formation of supramolecular polymers. Head-to-tail hydrogen bonding of the squaramide synthons was achieved when a carbamate moiety was included to link together hydrophilic and hydrophobic domains, unlike when an ether linkage was used. Neither FMN or $Ru(Bpy)^{3+}$ photoinitiators resulted in the formation of tyrosine crosslinks after visible light irradiation at various monomer concentrations. These results suggest that the tyrosine moiety may be inaccessible to the photoinitiator for crosslinking, and thus further optimization with respect to the monomer or photocrosslinking conditions is required to enable dityrosine formation to drive changes in the formed supramolecular polymers and materials.

References

1. Li, J.; Xing, R.; Bai, S.; Yan, X., Recent advances of self-assembling peptide-based hydrogels for biomedical applications. *Soft Matter* **2019**, *15*, 1704–1715.
2. Dasgupta, A.; Mondal, J. H.; Das, D., Peptide hydrogels. *RSC Adv.* **2013**, *3*, 9117-9149.
3. Webber, M. J.; Appel, E. A.; Meijer, E. W.; Langer, R., Supramolecular biomaterials. *Nat. Mater.* **2016**, *15*, 13–26.
4. Mondal, S.; Das, S.; Nandi, A. K., A review on recent advances in polymer and peptide hydrogels. *Soft Matter* **2020**, *16*, 1404–1454.
5. Diaferia, C.; Netti, F.; Ghosh, M.; Sibillano, T.; Giannini, C.; Morelli, G.; Adler-Abramovich, L.; Accardo, A., Bi-functional peptide-based 3D hydrogel-scaffolds. *Soft Matter* **2020**, *16*, 7006–7017.
6. Sun, B.; Ariawan, A. D.; Warren, H.; Goodchild, S. C.; In Het Panhuis, M.; Ittner, L. M.; Martin, A. D., Programmable enzymatic oxidation of tyrosine-lysine tetrapeptides. *J. Mater. Chem. B* **2020**, *8*, 3104–3112.
7. Lampel, A.; McPhee, S. A.; Park, H. A.; Scott, G. G.; Humagain, S.; Hekstra, D. R.; Yoo, B.; Frederix, P. W. J. M.; Li, T. De; Abzalimov, R. R.; Greenbaum, S. G.; Tuttle, T.; Hu, C.; Bettinger, C. J.; Ulijn, R. V., Polymeric peptide pigments with sequence-encoded properties. *Science,* **2017**, *356*,1064–1068.
8. Handelman, A.; Beker, P.; Amdursky, N.; Rosenman, G., Physics and engineering of peptide supramolecular nanostructures. *Phys. Chem. Chem. Phys.* **2012**, *14*, 6391–6408.
9. Lou, S.; Wang, X.; Yu, Z.; Shi, L., Peptide Tectonics: Encoded structural complementarity dictates programmable self-assembly. *Adv. Sci.* **2019**, *6*, 1802043, 1-24.
10. Adams, D. J., Dipeptide and tripeptide conjugates as low-molecular-weight hydrogelators. *Macromol. Biosci.* **2011**, *11*, 160–173.
11. Levin, A.; Hakala, T. A.; Schnaider, L.; Bernardes, G. J. L.; Gazit, E.; Knowles, T. P. J., Biomimetic peptide self-assembly for functional materials. *Nat. Rev. Chem.* **2020**, *4*, 615–634.
12. Draper, E. R.; Morris, K. L.; Little, M. A.; Raeburn, J.; Colquhoun, C.; Cross, E. R.; McDonald, T. O.; Serpell, L. C.; Adams, D. J., Hydrogels formed from Fmoc amino acids. *CrystEngComm* **2015**, *17*, 8047–8057.
13. Arakawa, H.; Takeda, K.; Higashi, S. L.; Shibata, A.; Kitamura, Y.;

Ikeda, M., Self-assembly and hydrogel formation ability of Fmoc-dipeptides comprising α-methyl-L-phenylalanine. *Polym. J.* **2020**, *52*, 923–930.
14. Liebmann, T.; Rydholm, S.; Akpe, V.; Brismar, H., Self-assembling Fmoc dipeptide hydrogel for in situ 3D cell culturing. *BMC Biotechnol.* **2007**, *7*, 1–11.
15. Arkenberg, M. R.; Nguyen, H. D.; Lin, C. C., Recent advances in bio-orthogonal and dynamic crosslinking of biomimetic Hydrogels, *J. Mater. Chem. B*, **2020**, 8, 7835-7855
16. Echalier, C.; Valot, L.; Martinez, J.; Mehdi, A.; Subra, G., Chemical cross-linking methods for cell encapsulation in hydrogels. *Mater. Today Commun.* **2019**, *20*, 100536, 1-44
17. Huang, S.; Kong, X.; Xiong, Y.; Zhang, X.; Chen, H.; Jiang, W.; Niu, Y.; Xu, W.; Ren, C., An overview of dynamic covalent bonds in polymer material and their applications. *Eur. Polym. J.* **2020**, *141*, 110094, 1-18
18. GhavamiNejad, A.; Ashammakhi, N.; Wu, X. Y.; Khademhosseini, A., Crosslinking strategies for 3D bioprinting of polymeric hydrogels. *Small* **2020**, *16* (35), 2002931, 1-30
19. Li, L.; Scheiger, J. M.; Levkin, P. A., Design and applications of photoresponsive hydrogels. *Adv. Mater.* **2019**, *31*, 1807333, 1-17
20. Hu, W.; Wang, Z.; Xiao, Y.; Zhang, S.; Wang, J., Advances in crosslinking strategies of biomedical hydrogels. *Biomater. Sci.* **2019**, *7*, 843–855.
21. Lee, J.; Ju, M.; Cho, O. H.; Kim, Y.; Nam, K. T., Tyrosine-rich peptides as a platform for assembly and material synthesis. *Adv. Sci.* **2019**, *6*, 1-15
22. Liu, H.-Y.; Nguyen, H. D.; Lin, C.-C., Dynamic PEG–peptide hydrogels via visible light and FMN-induced tyrosine dimerization. *Adv. Healthc. Mater.* **2018**, *7*, 1800954, 1-10.
23. Jang, H. S.; Lee, J. H.; Park, Y. S.; Kim, Y. O.; Park, J.; Yang, T. Y.; Jin, K.; Lee, J.; Park, S.; You, J. M.; Jeong, K. W.; Shin, A.; Oh, I. S.; Kwon, M. K.; Kim, Y. Il; Cho, H. H.; Han, H. N.; Kim, Y.; Chang, Y. H.; Paik, S. R.; Nam, K. T.; Lee, Y. S., Tyrosine-mediated two-dimensional peptide assembly and its role as a bio-inspired catalytic scaffold. *Nat. Commun.* **2014**, *5*, 1–11.
24. Min, K. I.; Yun, G.; Jang, Y.; Kim, K. R.; Ko, Y. H.; Jang, H. S.; Lee, Y. S.; Kim, K.; Kim, D. P., Covalent self-assembly and one-step photocrosslinking of tyrosine-rich oligopeptides to form diverse

nanostructures. *Angew. Chemie - Int. Ed.* **2016**, *55*, 6925–6928.
25. Partlow, B. P.; Bagheri, M.; Harden, J. L.; Kaplan, D. L., Tyrosine templating in the self-assembly and crystallization of silk fibroin. *Biomacromolecules* **2016**, *17*, 3570–3579.
26. Zhang, X.; Zhang, Y.; Chen, W.; Xu, L.; Wei, S.; Zheng, Y.; Zhai, M., Biological behavior of fibroblast on contractile collagen hydrogel crosslinked by γ-irradiation. *J. Biomed. Mater. Res. Part A* **2014**, *102*, 2669–2679.
27. Al, E.; Güçlü, G.; İyim, T. B.; Emik, S.; Özgümüş, S., Synthesis and properties of starch-graft-acrylic acid/Na-montmorillonite superabsorbent nanocomposite hydrogels. *J. Appl. Polym. Sci.* **2008**, *109*, 16–22.
28. Rosales, A. M.; Anseth, K. S., The design of reversible hydrogels to capture extracellular matrix dynamics. *Nat. Rev. Mater.* **2016**, *1*, 15012, 1-15.
29. Tong, C.; Wondergem, J. A. J.; Heinrich, D.; Kieltyka, R. E., Photopatternable, branched polymer hydrogels based on linear macromonomers for 3D cell culture applications. *ACS Macro Lett.* **2020**, *9*, 882–888.
30. Tong, C.; Liu, T.; Saez Talens, V.; Noteborn, W. E. M.; Sharp, T. H.; Hendrix, M. M. R. M.; Voets, I. K.; Mummery, C. L.; Orlova, V. V; Kieltyka, R. E., Squaramide-based supramolecular materials for three-dimensional cell culture of human induced pluripotent stem cells and their derivatives. *Biomacromolecules* **2018**, *19*, 1091–1099.
31. Liu, T.; van den Berk, L.; Wondergem, J. A. J.; Tong, C.; Kwakernaak, M. C.; Braak, B. ter; Heinrich, D.; van de Water, B.; Kieltyka, R. E., Squaramide-based supramolecular materials drive HepG2 spheroid differentiation. *Adv. Healthc. Mater.* **2021**, *10*, 2001903, 1-10.
32. Pandya, D. N.; Pailloux, S.; Tatum, D.; Magda, D.; Wadas, T. J., Di-macrocyclic terephthalamide ligands as chelators for the PET radionuclide zirconium-89. *Chem. Commun.* **2015**, *51*, 2301–2303.
33. Liu, H. Y.; Nguyen, H. D.; Lin, C. C., Dynamic PEG–peptide hydrogels via visible light and FMN-induced tyrosine dimerization. *Adv. Healthc. Mater.* **2018**, *7*, 1–10.
34. Edwards, A. M., Structure and general properties of flavins. In *Flavins and Flavoproteins: Methods and Protocols*; Weber, S., Schleicher, E., Eds.; Springer New York: New York, NY, 2014; 3–13.
35. Holzer, W.; Shirdel, J.; Zirak, P.; Penzkofer, A.; Hegemann, P.; Deutzmann, R.; Hochmuth, E., Photo-induced degradation of some

flavins in aqueous solution. *Chem. Phys.* **2005**, *308*, 69–78.
36. Edwards, A. M.; Bueno, C.; Saldaño, A.; Silva, E.; Kassab, K.; Polo, L.; Jori, G., Photochemical and pharmacokinetic properties of selected flavins. *J. Photochem. Photobiol. B Biol.* **1999**, *48*, 36–41.
37. Görner, H., Oxygen uptake after electron transfer from amines, amino acids and ascorbic acid to triplet flavins in air-saturated aqueous solution. *J. Photochem. Photobiol. B Biol.* **2007**, *87*, 73–80.
38. Zhang, X.; Wu, X.; Jiang, S.; Gao, J.; Yao, Z.; Deng, J.; Zhang, L.; Yu, Z., Photo-accelerated "click" reaction between diarylsydnones and ring-strained alkynes for bioorthogonal ligation. *Chem. Commun.* **2019**, *55*, 7187–7190.

SUPPORTING INFORMATION

5.5 Materials and methods

5.5.1 Materials

All reagents and chemicals were purchased from Sigma Aldrich, Acros Organics and Bioconnect, and used without further purification. Deuterated chloroform was purchased from Euriso-top and Milli-Q water was employed for all experiments. Acetonitrile for the hydrogenation reaction was dried by molecular sieves 3Å (20 % w/v) and used after 24h. Compound **5a** was synthesized as previously reported.[38]

5.5.2 Methods

Compounds were either purified by silica gel column chromatography or on X1 flash chromatography system equipped with a C18 column from Grace Reveleris using a gradient of H_2O/CH_3CN. ^{1}H-NMR and ^{13}C spectra were obtained on a Bruker (300 MHz) or Bruker DMX-400 (400 MHz). LC-MS analysis was performed on a Finnigan Surveyor HPLC system equipped with a Gemini C18 50 x 4.60 mm column (UV detection at 254 and 214 nm) coupled to Finnigan LCQ Advantage Max mass spectrometer with ESI. For the mobile phase, a gradient of 10-90% of CH_3CN/H_2O with 0.1% trifluoroacetic acid over 13.5 minutes was used. MALDI-TOF-MS spectra were obtained on a Bruker Microflex LRF mass spectrometer in relfection positive mode using α-cyano-4-hydroxycinnamic acid with a laser power of 30%. UV-vis measurements were performed on a Cary 300 UV-vis spectrophotometer using a quartz cuvette of 1 cm path length. The High resolution mass spectra (HR-MS) were collected on a Thermo Fisher LTQ Orbitrap mass spectrometer equipped with an electrospray ion source in positive mode (resolution R = 60000). The spectra were obtained by direct injection (2 µL) of samples (1 µM in H2O-CH_3CN 50/50 v/v) via Ultimate 3000 nano UPLC (Dionex) system with an external calibration (Thermo Scientific) and recorded with a mass range of 150-2000. DLS measurements were carried out using a Malvern Zetasizer Nano ZS ZEN3500 equipped with a laser of 633 nm at a scattering angle of 173°. Atomic force microscopy (AFM) images were recorded in a tapping mode on a Veeco Multimode AFM with a Nanoscope IIIa controller device at room temperature and processed

using the Nanoscope software. Atomic force microscopy (AFM) images were recorded in tapping mode on a Veeco-Bruker Multimode AFM with a Nanoscope IIIa controller at room temperature. The AFM tips used were Oltespa Opus probes with a reflex aluminium coating, with a nominal spring constant of 2 N/m, a nominal resonance frequency of 70 kHz and a tip radius of 7 nm. The images were processed using Nanoscope software. Fluorescence experiments were recorded on an Aqualog Horiba Scientific fluorimeter with a quartz cuvette of 10 mm. The mechanical properties of the squaramide-based hydrogels were measured on a Discovery HR-2 hybrid rheometer with a Peltier-based temperature controller and a solvent trap. The cone-plate geometry (40 mm, 1.995°) was used and the pre-made hydrogel (600 µL) were gently pipetted into the lower plate. The gap was set at 54 µm. The sample was covered with the oil to avoid the drying during the measurement. The temperature ramp experiment was performed starting from 25 °C and ending at 85 °C with the constant ramp rate at 1 °C/min. The measurement was performed at a fixed frequency (1 Hz) and strain (0.05%).

5.7 Synthetic routes

5.7.1 Synthesis of 2

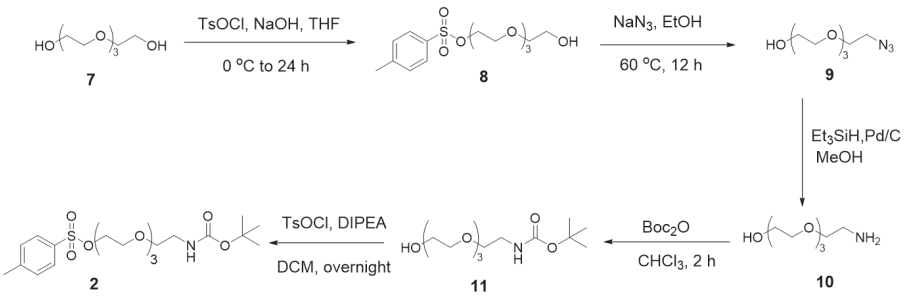

Scheme S1: Synthetic route for molecule **2.**

Synthesis of 8

Tetraethylene glycol (20.0 g, 0.1 mol), was dissolved in DCM (300 mL) and Et_3N (2.09 mL, 0.015 mol) was added. The reaction mixture was cooled down at 0 °C and a solution of tosyl chloride (1.96 g, 0.010 mol) was added dropwise in 2h and stirred overnight at RT. The reaction mixture was concentrated by rotary evaporation and was redissolved in DCM (200 mL). The organic layers were washed with water (3x 200 mL), dried with $MgSO_4$ and concentrated by rotary evaporation yielding as a colorless oil.

Yield: 25 g, 71.7%. ^{1}H NMR (300 MHz, $CDCl_3$) δ 6.75 – 6.66 (m, 2H), 6.32 – 6.23 (m, 2H), 4.25 (s, 3H), 3.12 – 3.02 (m, 2H), 2.68 – 2.52 (m, 9H), 2.49 (m, 7H), 2.19 – 2.07 (m, 1H), 1.36 (s, 3H). ^{13}C NMR (75 MHz, $CDCl_3$) δ 143.83, 131.75, 129.88, 126.38, 76.76, 76.33, 75.90, 71.70, 71.44, 69.51, 69.46, 69.35, 69.28, 69.15, 68.86, 68.30, 67.49, 60.40, 52.61, 44.95, 20.49.

Synthesis of 9

8 (3.12g, 8.97 mmol) was dissolved in DMF (20 mL) and NaN_3 was added. The reaction mixture was refluxed overnight at 60 °C. The solvent was removed by rotary evaporation and the residue was redissolved in water (20 mL) and extracted with EtOAc (3 x 20 mL). The organic layers were dried with $MgSO_4$ and concentrated by rotary evaporation. The compound was

purified by chromatographic silica colum (EtOAc 100%, EtOAc/PE 9/1) and isolated as a yellowish oil.

Yield: 0.770g, 40%. ^{1}H NMR (300 MHz, $CDCl_3$) δ (ppm): 3.63 – 3.50 (m, 11H), 3.47 (m, 2H), 3.27 (t, 2H). ^{13}C NMR (75 MHz, $CDCl_3$) δ (ppm): 162.55, 77.75, 77.33, 76.90, 72.46, 70.52, 70.47, 70.41, 70.17, 69.89, 61.42, 50.50.

Synthesis of 10

9 (0.770 g, 3.5 mmol) was dissolved in dry MeOH (10 mL) and Pd/C (0.186 g, 1.75 mmol) was added under N_2 atmosphere. Et_3SiH (17 mL, 105 mmol) was added dropwise and the mixture was stirred overnight. After the filtration on celite, the residue was isolated removing the solvent under a gentle stream of N_2 gas. The reaction was quantitative and the compound was isolated as a yellowish oil.

^{1}H NMR (400 MHz, $CDCl_3$) δ (ppm): 3.77 – 3.46 (m, 20H), 2.90 – 2.74 (m, 2H). ^{13}C NMR (75 MHz, $CDCl_3$) δ 163.42, 77.88, 77.45, 77.02, 72.60, 72.36, 71.34, 71.04, 70.88, 70.38, 70.25, 70.20, 70.12, 69.97, 69.91, 69.87, 69.83, 69.76, 69.42, 62.02, 60.87, 60.77, 48.60, 42.55, 41.18, 40.59.

Synthesis of 11

10 (0.841g, 4.35 mmol) was dissolved in EtOH (20 mL) and Boc_2O (1.04g, 94.78 mmol) was added to the reaction mixture and stirred at RT for 2h. After the removal of the solvent by rotary evaporation, the crude was redissolved in DCM, washed with water (2 x 20 mL), and dried with $MgSO_4$. The organic layers were concentrated and the compound, isolated as a white powder, was used for next step without further purification.

^{1}H NMR (300 MHz, $CDCl_3$) δ (ppm): 3.74 (m, 2H), 3.58 – 3.42 (m, 12H), 3.22 (m, 2H), 1.42 (s, 9H). ^{13}C NMR (75 MHz, $CDCl_3$) δ (ppm): 156.14, 77.57, 77.14, 76.72, 72.60, 72.53, 70.63, 70.56, 70.54, 70.48, 70.37, 70.32, 70.27, 70.18, 70.14, 70.02, 69.53, 62.20, 61.51, 40.30, 28.47, 4.30.

Synthesis of 2

11 (1.17g, 3.98 momol) was dissolved in DCM (20 mL) and tosyl chloride (0.91 g, 4.78 mmol), trimethylamine (0.832 mL, 5.97 mmol) and a catalytic amount of 4-(dimethylamino)-piperidine (0.024 g, 0.199 mmol) were added.

The reaction mixture that was stirred overnight at RT. Subsequently, water (20 mL) was added to the reaction mixture and the aqueous layers were extracted with DCM (3 x 20 mL). The organic layers were combined and dried with $MgSO_4$ and concentrated by rotary evaporation. The crude was purified by chromatographic silica column (DCM/MeOH 95/5) and the product was obtained as a colorless oil. LCMS (t= 7.12 min, (m/z): 469.44 $[M+Na]^+$

Yield: 1.5g, 84.2%. ^{1}H NMR (400 MHz, $CDCl_3$) δ (ppm): 7.83 (d 2H), 7.37 (d, 2H), 4.18 (m, 2H), 3.83 – 3.42 (m, 21H), 3.37 – 3.29 (m, 2H), 2.48 (s, 3H), 1.47 (s, 9H). ^{13}C NMR (101 MHz, $CDCl_3$) δ (ppm) = 145.08, 129.84, 127.27, 77.39, 77.07, 76.76, 72.69, 70.78, 70.57, 70.53, 70.23, 69.25, 68.71, 62.28, 40.35, 28.43, 20.70, 4.37.

5.7.2 Synthesis of 6

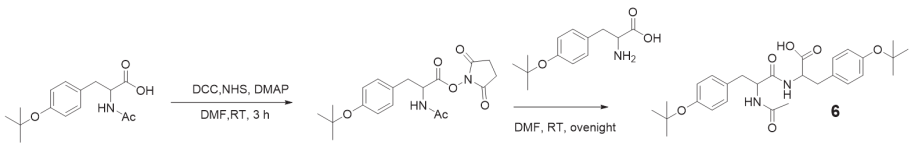

Scheme S2: Synthetic route for protected dityrosine **6**.

Acetyl-O-(tert-butyl)-L-tyrosine (0.600 g, 2.14 mmol) was dissolved in dry DMF (10 mL) and N,N-dicyclohexylcarbodiimide (0.529 g, 2.57 mmol) and 4-dimethylaminopyridine (DMAP) (0.026 g, 0.214 mmol) were stirred for 20 min at RT. N-hydroxysuccinimide (0.320 g, 2.57 mmol) was added and the mixture was stirred for an additional 3 h. Subsequently O-tert-butyl-L-tyrosine was added and the reaction mixture was stirred overnight. The crude was filtered and the solvent was removed under vacuum. EtOAc was added to the residue and filtered a second time to remove DCU. The organic layer was washed with water (3x) and dried with $MgSO_4$. The compound was purified by flash chromatography using H_2O/CH_3CN (10-90 %) over 40 min and was obtained as a colorless oil.

Yield: 0.8 g, 75%.^{1}H NMR (300 MHz, $CDCl_3$): δ (ppm) =7.08 – 6.95 (m, 2H), 6.81 (m, 3H), 3.55 (m, 1H), 3.21 – 2.75 (m, 4H), 1.89 (d, 3H), 1.34 – 1.19 (m, 18H). ^{13}C NMR (75 MHz, $CDCl_3$): δ (ppm) = 175.00, 174.54, 170.20, 169.89, 169.77, 169.72, 153.99, 153.94, 153.67, 153.56, 132.99, 132.93, 131.88, 131.64, 130.22, 130.16, 129.48, 123.05, 121.23, 78.22, 78.06, 77.51, 77.09,

76.67, 55.95, 54.39, 41.08, 37.99, 37.72, 37.40, 37.09, 28.80, 21.84. LC-MS: t= 6.71 min, (m/z): 499.50 $[M]^+$, HRMS (m/z): 499.00 $[M]^+$.

5.7.3 Synthesis of 1a and 1b

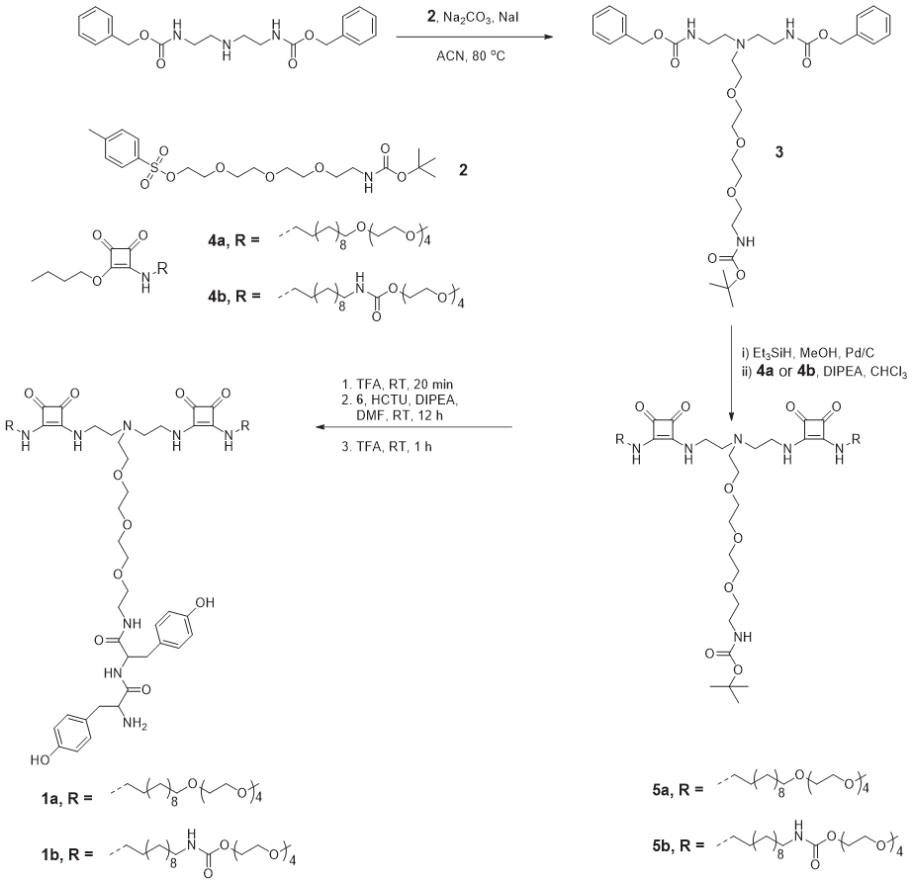

Scheme S3: Synthetic route for molecule **1a** and **1b**.

Synthesis of 3

N,N-Di-Z-diethylenetriamine (0.230 g, 0.62 mmol) was dissolved in anhydrous CH_3CN, and successively, K_2CO_3 (0.128 g, 0.93 mmol), 5 (0.513 g, 1,15 mmol) and NaI (0.096 g, 0.64 mmol) were added and refluxed for 36 h. Subsequently, the solvent was removed under vacuum and the crude was

redissolved in DCM. The organic layers were washed 3x times with NaOH 1 M and were dried with Na_2SO_4. The compound was purified by flash chromatography using a gradient of H_2O/CH_3CN 10-90% over 40 min and was obtained as a white powder.

Yield: 0.126g, 31.4 % ^{1}H NMR (400 MHz, $CDCl_3$): δ (ppm) = 7.33 (m, 10H), 5.98 (s, 2H), 5.08 (s, 4H), 3.75 – 3.39 (m, 13H), 3.25 (m, 6H), 2.65 (m, 6H), 1.46 (s, 9H). ^{13}C NMR (100 MHz, $CDCl_3$): δ (ppm) = δ 156.81, 156.02, 136.86, 128.34, 128.06, 79.15, 77.46, 77.14, 76.83, 71.99, 70.44, 70.24, 70.14, 69.87, 66.48, 54.29, 53.29, 40.31, 39.17. LC-MS: t= 6.45 min, (m/z): 646.50 $[M]^+$, MALDI (m/z): 646.50 $[M+H]^+$.

Synthesis of 5a

3 (0.287 g, 0.430 mmol) was dissolved in dry MeOH (6 mL) and Pd/C (0.5 eq, 0.215 mmol, 0.023 g) was added. The reaction mixture was placed under a nitrogen atmosphere and Et_3SiH (20 eq, 5.74 mmol, 0.916 mL) was added dropwise prior to stirring the reaction overnight. The deprotection was verified by LCMS (t= 3.55 min, m/z: 378.14 $[M]^+$). Subsequently, the reaction mixture was filtered over celite and the solvent was removed by a gentle stream of N_2. The residue (0.189 g, 0.5 mmol) was redissolved in $CHCl_3$, and **4a**, (0.592 g, 1.15 mmol) or **4b** (0.62 g, 1.1 mmol) and DIPEA (3 eq, 1.5 mmol, 0.262 mL) were added and refluxed overnight. The crude was extracted with water (3x 20 mL) and dried by Na_2SO_4. The compound was purified on a silica column chromatography (EtOAc 100%, DCM/ MeOH (95:5) to obtain the compound **5a** as a white solid.

5a: Yield: 0.18g. 30 %, ^{1}H NMR (300 MHz, $CDCl_3$): δ (ppm) = 3.68 – 3.61 (m, 38H), 3.61 – 3.50 (m, 13H), 3.44 (m, 5H), 3.38 (s, 6H), 3.29-3.23 (m, 2H), 2.07 (s, 5H), 1.64 (m, 4H), 1.57 (m, 4H), 1.44 (s, 9H), 1.39 – 1.22 (m, 26H). ^{13}C NMR (75 MHz, $CDCl_3$): δ (ppm) = 182.67, 181.92, 168.72, 167.24, 156.00, 77.52, 77.09, 76.67, 71.85, 71.51, 70.52, 70.47, 70.40, 70.25, 69.99, 69.95, 58.99, 44.59, 42.49, 40.23, 31.12, 29.58, 29.47, 29.27, 28.41, 26.55, 26.05. MALDI (m/z): 1283.03 $[M+H]^+$.

Synthesis of 5b

3 (200 mg, 0.3 mmol) was dissolved in dry MeOH (5 mL) and Pd/C (64 mg, 0.215 mmol) was added. The reaction mixture was placed under a nitrogen atmosphere and triethylsilane (500 µL, 3.09 mmol) was added dropwise for

30 min and stirred for 2 hrs. The deprotection was verified by LC-MS (t= 3.19 min, m/z: 379.33 $[M]^+$). Subsequently, the reaction mixture was filtered over celite and washed with methanol. The solvent was removed through rotavapor. The residue was redissolved in $CHCl_3$, and **4b** (168 mg, 0.6 mmol) and DIPEA (46 µL, 0.264 mmol) were added and refluxed overnight. The crude was purified through silica column chromatography (MeOH/DCM = 2:8) and removed the solvent to obtain the compound **5b** as a white solid.

5b: Yield: 0.18g. 30 %, ^{1}H NMR (300 MHz, $CDCl_3$): δ (ppm) = 3.68 – 3.61 (m, 38H), 3.61 – 3.50 (m, 13H), 3.44 (m, 5H), 3.38 (s, 6H), 3.29-3.23 (m, 2H), 2.07 (s, 5H), 1.64 (m, 4H), 1.57 (m, 4H), 1.44 (s, 9H), 1.39 – 1.22 (m, 26H). ^{13}C NMR (75 MHz, $CDCl_3$): δ (ppm) = 182.67, 181.92, 168.72, 167.24, 156.00, 77.52, 77.09, 76.67, 71.85, 71.51, 70.52, 70.47, 70.40, 70.25, 69.99, 69.95, 58.99, 44.59, 42.49, 40.23, 31.12, 29.58, 29.47, 29.27, 28.41, 26.55, 26.05. LCMS: t= 6.19 min, m/z: 1369.15 $[M+Na]^+$.

Synthesis of 1a

5a (0.144 mmol, 0.167 g) was dissolved in TFA and stirred at RT for 20 min to remove the boc protecting group. Afterwards, the TFA was removed by a gentle stream of N_2 and the reaction was dissolved in 10 mL of DMF and HCTU (0.268 g, 0.648 mmol), **6** (0.358 g, 0.719 mmol) and DIPEA (0.250 mL,1.44 mmol) were added and stirred overnight. The solvent was removed under vacuum and purified by flash chromatography using a gradient of H_2O/CH_3CN from 10-90 % over 40 min. The tert-butyl group of dityrosine was then removed using TFA (3 mL) in 1 h at RT and the compound **1a** was purified by flash chromatography on a C18 silica column using a gradient of H_2O/CH_3CN 10-90 % over 35 minutes. The final compound was obtained as a colorless sticky oil.

1a: Yield: 0.100 g, 57 % ^{1}H NMR (400 MHz, $CDCl_3$): δ (ppm) = 8.50 (s, 2H), 6.95-6.6 (m, 9H), 3.67 – 3.59 (m, 31H), 3.59 – 3.51 (m, 13H), 3.50 – 3.39 (m,13H), 3.36 (s, 6H), 2.84 (s, 4H), 2.40 (s, 4H), 1.87 (s, 2H), 1.67-1.50 (m, 9H), 1.37 – 1.19 (m, 27H).^{13}C NMR (100 MHz, $CDCl_3$): δ (ppm) = 181.97, 146.91, 128.81, 128.71, 127.99, 127.32, 77.40, 77.08, 76.76, 71.85, 71.59, 70.48, 70.43, 70.39, 70.34, 69.92, 59.01, 30.94, 29.57, 29.49, 29.27, 26.48, 26.05. LC-MS: t= 6.04 min, (m/z): 1529.4 $[M+H]^+$, MALDI (m/z): 1567 $[M+K]^+$.

Synthesis of 1b

5b (10 mg, 7.4 mmol) was dissolved in 50% DCM/TFA and stirred at room temperature for 2 hr. The deprotection was verified by LCMS (t= 5.31 min, m/z: 1269.18 $[M+Na]^+$). Afterwards, the TFA was removed by a gentle stream of N_2 and the reaction was dissolved in 10 mL of chloroform and NHS activated dityrosine (**6)** (9 mg, 14.8 mmol) and DIPEA (13 µL, 74.2 mmol) were added and stirred overnight. The solvent was removed under vacuum. The formation of product was characterized by LC-MS ((t= 6.12 min, m/z: 1728.08 $[M+H]^+$). The tert-butyl group in the dityrosine part was then removed using 50% DCM/TFA (10 mL) in 2 h at RT and the compound **1b** was purified by reverse phase HPLC on a C18 silica column using a gradient of H_2O/CH_3CN 10-90 % over 20 minutes.

1b: Yield: 0.100 g, 30 %. ^1H NMR (300 MHz, $CDCl_3$): δ (ppm) = 8.9 (s, 2H), 6.92 (m, 4H), 6.83 (m, 4H), 4.92 (t, 2H), 4.2 (m, 4H), 3.69 – 3.52 (m, 36H), 3.41 (s, 6H), 3.35 (m, 16H) 3.18 (m, 6H), 2.51 (m, 6H), 1.84 (s, 3H), 1.5 – 1.28 (m, 32H). LC-MS: t= 5.92 min, (m/z): 1614.12 $[M]^+$.

5.7.1 Characterization

Sample preparation

A stock solution of compound **1a** in DMSO at concentration of 1 mM was prepared and the solvent was removed by a stream of N_2. The solution was rehydrated with water at a concentration of 1 mM. Subsequently, aliquots from the stock solution were taken to prepare solutions at the desired concentration for solution phase measurements and used as is for gel phase experiments. All samples were left to stand overnight before measurement.

For samples using the photoinitiator riboflavin 5'-mononucleotide (FMN), a stock solution of FMN was prepared at 10 mM. An aliquot of the photoinitiator solution was diluted in presence of **1a** (1 mM) to provide a final concentration of 1 mM. After irradiation at 440 nm, aliquots from the stock solution were taken to prepare solutions at the desired concentration for solution phase measurements.

Photo-crosslinking of **1b** was performed using a stock solution of **1b** (1 mM), $[Ru(bpy)_3]^{2+}$ (2.2 mM) and SPS (22 mM). The sample containing **1b** in self-assembled state (0.166 mM) in the presence of $[Ru(bpy)_3]^{2+}$ and SPS was photoirradiated using visible light (λ = 450 nm).

UV-vis spectroscopy

Solutions of **1a** at 15 μM concentration in water were prepared as described according to the sample preparation protocol above. The samples were placed in the UV-vis and a spectrum was recorded from 200-500 nm. The solutions were prepared in triplicate and for each solution the UV-vis spectra was measured.

The solutions containing the photoinitiator, as described in the protocol above, were irradiated at 440 nm at different times (5, 10, 15, 20 25, 60 and 120 min). Subsequently, aliquots from the stock were taken to prepare solutions at 15 μM and were equilibrated overnight prior the measurements. The samples were placed in the UV-vis and a spectrum was recorded from 200-500 nm. The solutions were prepared in triplicate and for each solution the UV-vis spectra was measured.

In the case of **1b**, absorption changes were measured after photoirradiation at 450 nm in the presence of photoinitiator ($[Ru(bpy)_3]^{2+}$ and SPS). The photoirradiation and absorption changes at high concentrations were performed using 1 mm cuvette. The baseline correction was carried out using blank containing photoinitiator at the similar concentrations.

Fluorescence measurements

Solutions of **1a** (1 mM) in presence of FMN (1 mM) were prepared in different vials and irradiated at different times (5, 10, 15, 20 25, 60 and 120 min) with visible light at 330 nm. Subsequently, aliquots from the stock solutions were taken to prepare solutions a at 15 μM concentration for measurement. Fluorescence spectra were recorded using an excitation wavelength at 330 nm and the emission spectra were recorded from 350 to 620 nm at RT.

Critical aggregation concentration determination

A stock solution of **1a** at 1 mM concentration was prepared and equilibrated overnight. The stock solution was diluted to several concentrations between 100 μM to 10 nM and equilibrated for at least 3h prior to measurement of scattering intensity. Each measurement was carried out using a disposable DLS cuvette and performed in triplicate. The data was plotted using the scattering intensity as a function of log [C]. The critical aggregation concentration was then determined from the intersection of the two lines drawn through the points collected for the scattering intensities collected at the various concentrations.

Atomic force microscopy (AFM)

A solution of **1a** was prepared according to the preparation protocol above at a concentration of 15 μM and equilibrated overnight. An aliquot (25 μL) of this solution was pipetted on cleaved mica and dried overnight at RT before the measurement. The analysis of AFM images was performed using the Nanoscope software.

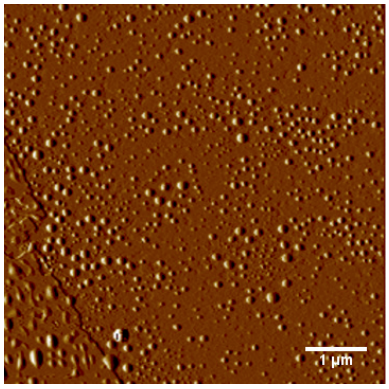

Figure S5.1 AFM micrograph of **1a** (amplitude) (scale bar: 1 µm).

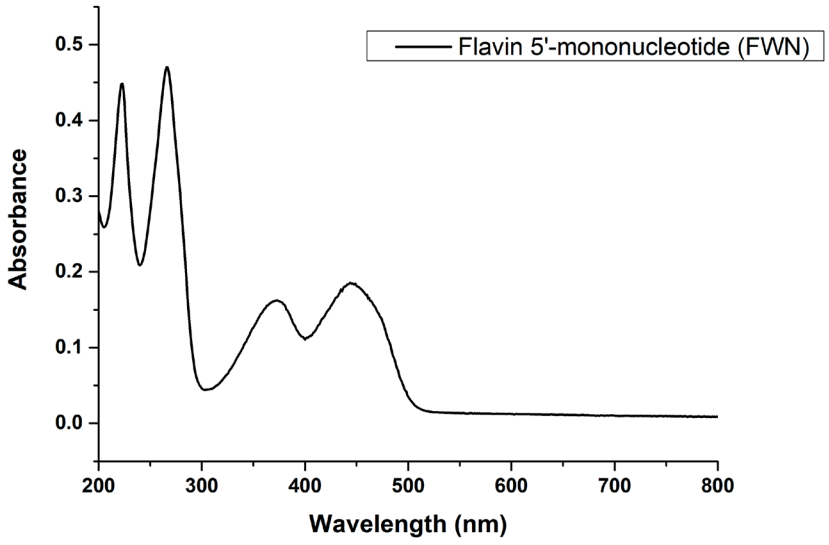

Figure S5.2 UV-vis spectra of FMN at 15 µM

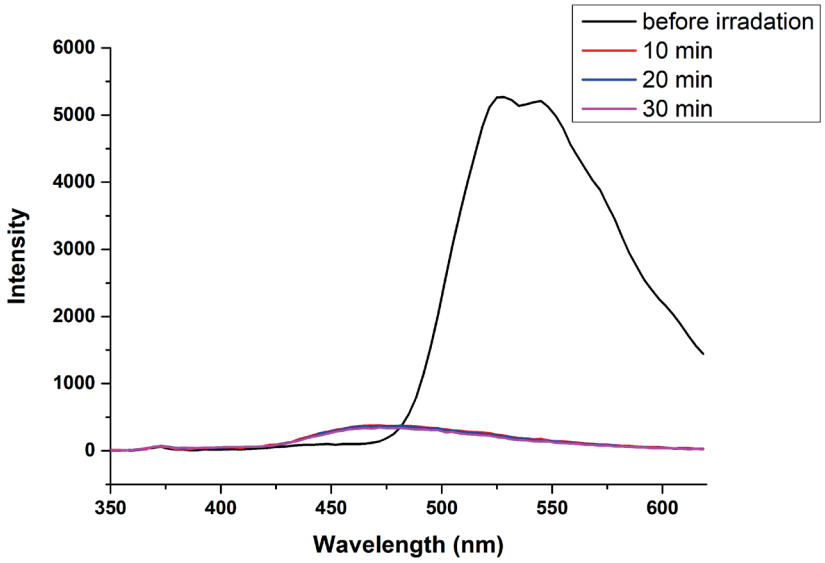

Figure S5.3 Emission spectra of FMN at 15 μM after different visible light irradiation times (10, 20 and 30 min).